American Journal of Transplantation 2016; 16: 99–110
Wiley Periodicals Inc.

doi: 10.1111/ajt.13421

RNA Profiling in Human and Murine Transplanted Hearts: Identification and Validation of Therapeutic Targets for Acute Cardiac and Renal Allograft Rejection

L. N. L. Van Aelst[1], G. Summer[2], S. Li[3], S. K. Gupta[4], W. Heggermont[1], K. De Vusser[5], P. Carai[1,2], M. Naesens[5], J. Van Cleemput[1], F. Van de Werf[1], J. Vanhaecke[1], T. Thum[4], M. Waer[3], A.-P. Papageorgiou[1,2], B. Schroen[2] and S. Heymans[1,2,6,*]

[1]*Department of Cardiovascular Sciences, University of Leuven, Leuven, Belgium*
[2]*Center for Heart Failure Research, Cardiovascular Research Institute Maastricht (CARIM), University Hospital Maastricht, Maastricht, the Netherlands*
[3]*Laboratory of Experimental Transplantation, University of Leuven, Leuven, Belgium*
[4]*Institute of Molecular and Translational Therapeutic Strategies (IMTTS), Hannover Medical School, Hannover, Germany*
[5]*Department of Nephrology and Renal Transplantation, University Hospitals Leuven, Leuven, Belgium*
[6]*ICIN-Netherlands Heart Institute, Utrecht, the Netherlands*
[*]*Corresponding author: Stephane Heymans, s.heymans@maastrichtuniversity.nl*

Acute cellular rejection (ACR) is the adverse response of the recipient's immune system against the allogeneic graft. Using human surveillance endomyocardial biopsies (EMBs) manifesting ACR and murine allogeneic grafts, we profiled implicated microRNAs (miRs) and mRNAs. MiR profiling showed that miR-21, -142-3p, -142-5p, -146a, -146b, -155, -222, -223, and -494 increased during ACR in humans and mice, whereas miR-149-5p decreased. mRNA profiling revealed 70 common differentially regulated transcripts, all involved in immune signaling and immune-related diseases. Interestingly, 33 of 70 transcripts function downstream of IL-6 and its transcription factor spleen focus forming virus proviral integration oncogene (SPI1), an established target of miR-155, the most upregulated miR in human EMBs manifesting rejection. In a mouse model of cardiac transplantation, miR-155 absence and pharmacological inhibition attenuated ACR, demonstrating the causal involvement and therapeutic potential of miRs. Finally, we corroborated our miR signature in acute cellular renal allograft rejection, suggesting a nonorgan specific signature of acute rejection. We concluded that miR and mRNA profiling in human and murine ACR revealed the shared significant dysregulation of immune genes. Inflammatory miRs, for example miR-155, and transcripts, in particular those related to the IL-6 pathway, are promising therapeutic targets to prevent acute allograft rejection.

Abbreviations: ACR, acute cellular rejection; EMB, endomyocardial biopsy; Gbp, guanylate-binding proteins; HF, heart failure; HTX, heart transplantation; ISH, *in situ* hybridization; ISHLT, International Society of Heart and Lung Transplantation; miR, microRNA; POD, postoperative day; SOCS1, suppressor of cytokine signaling 1; SPI1, spleen focus forming virus proviral integration oncogene; Tap, transporter associated with antigen processing; Trac, TCRα subunit constant gene; UTR, 3′ untranslated region

Received 25 January 2015, revised 22 May 2015 and accepted for publication 11 June 2015

Introduction

Heart transplantation (HTX) is the only curative treatment available for end-stage heart failure (HF). Despite contemporary immunosuppressive regimens, ACR occurs in approximately one quarter of recipients during the first year and accounts for 10% of deaths between 1 month and 1 year following transplantation (1). Furthermore, ACR is a risk factor for 5-year posttransplant mortality and cardiac allograft vasculopathy, the latter itself a major impediment to survival beyond 3 years after transplantation (1). Surveillance endomyocardial biopsies (EMBs) are the standard of care to diagnose acute rejection before graft function declines based on histopathological evidence of inflammation and cardiomyocyte necrosis; the International Society of Heart and Lung Transplantation (ISHLT) issues guidelines to standardize pathology reports (2). Despite decreasing rates of ACR due to improved immunosuppressants (1), new insights into the cellular changes associated with ACR remain important to diagnose ACR earlier, to identify patients at risk for ACR and to develop novel therapeutics without side effects (3).

In the past decade, miRs emerged as a popular gene family to serve as a target in a wide range of pathologies including

cardiovascular diseases. MiRs are phylogenetically conserved, noncoding RNAs which inhibit mRNA translation to protein by interacting with its 3′ untranslated region (UTR) (4). They are essential for cardiac development and homeostasis; miRs are also crucially involved in cardiac fibrosis, hypertrophy, and electrical remodeling (5). Several reports demonstrated altered serological and tissular miR expression following rejection of cardiac (6,7), hepatic (8), renal (9–11), and intestinal (12,13) allografts, yet these studied only one species, restricted the analysis to miR profiling without mRNA profiling and did not include a therapeutic intervention to demonstrate a causal role for specific miRs. One very recent report implicated miR-155 in murine cardiac allograft rejection through its interaction with suppressor of cytokine signaling 1 (SOCS1) in dendritic cells. Apart from not including a translation to human medicine, this study lacked unbiased miR and mRNA expression analysis (14).

In our study, we first determined common differentially expressed miRs and mRNAs in human ACR and a mouse model of ACR. Next, we unraveled mRNA pathways involved in ACR despite optimal therapy. Notably, the IL-6 pathway was markedly induced. MiR-155 expression was strongly upregulated in both humans and mice and its targeted genomic deletion or pharmacological inhibition attenuated inflammation and improved graft survival in a murine model. We concluded that RNA targeting, in particular miR-155 and the IL-6 functional pathway more specifically, represent an attractive novel treatment option for ACR.

Materials and Methods

Animals and surgery

Experiments were approved by the ethical committee of the KULeuven (Leuven, Belgium) and performed according to the Belgian legislation on laboratory animals. Eight to ten-week old BALB/cJ (Janvier), C57Bl/6J (Janvier), $bic^{m2/m2}$ (miR155−/−) and WT littermates (miR155+/+) were subjected to cervical heterotopic HTX and sham operations (15,16).

Human endomyocardial biopsies

Human material was obtained during sampling for clinical purposes and available for research according to the Declaration of Helsinki and the ethical committees at UZ Leuven (Leuven, Belgium) and Maastricht University Medical Center (Maastricht, the Netherlands). Surveillance EMBs included in our analyses were preferentially taken later than 6 weeks after transplantation to avoid the perioperative phase. Control biopsies consisted of age-matched patients with unexplained ventricular tachyarrhythmias yet with a normal ejection fraction, cardiac morphology, and no systemic or cardiac inflammation or viral persistence. Biopsies were snap-frozen for RNA analysis and formalin or Bouin fixed for histology.

Histological and morphometrical analysis

Mice were sacrificed 3, 5, or 7 days after HTX. Organs were removed, rinsed, blotted dry, weighed, and snap frozen. Before weighing, atria were separated from the ventricles. Ventricles were divided in basal, midventricular, and apical parts. The apical part was split and snap frozen. The midventricular part was used for *in situ* hybridization (ISH). The basal part was fixed in 4% paraformaldehyde (PFA; Sigma, Diegem, Belgium) in phosphate-buffered saline (PBS) overnight, post-fixed in ethanol, dehydrated, and embedded in paraffin. Four micrometer thick sections were made for histological (hematoxylin-eosin) and immunohistochemical stainings (17). Immunohistochemical stainings were performed with antibodies directed against CD45 (BD Biosciences, Erembodegem, Belgium), CD3 (AbD Serotec, Kidlington, UK), Mac3 (BD Biosciences). Omission of the primary antibody served as negative control.

In situ hybridization

The midventricular part of the harvested tissue was fixed in 10% neutral buffered formalin for 48 h, postfixed in ethanol, dehydrated, and embedded in paraffin. ISH was performed as described previously (18). Briefly, sections were dewaxed, dehydrated, air-dried, and incubated in 1.3 mg/mL Pepsin/0.1 mM HCl solution for 5 min at 37°C. Following a wash in MQ, sections were incubated at 42.5°C overnight in 1× hybridization buffer (ENZO Life Sciences, Antwerpen, Belgium) with 100 nM mmu-miR-155 double DIG-labeled probe or scrambled control (Exiqon). Afterwards, sections were washed in 5xSSC and in 0.2×SSC at hybridization temperature. Subsequently, sections were blocked in DIG blocking buffer from the DIG Wash and Block Buffer Set (Roche, Vilvoorde, Belgium) for 20 min followed by incubation in 1:500 anti-DIG-AP, Fab fragments (Roche) for 45 min. Sections were washed 3 × 5 min with TBS and incubated 3 min in DIG detection buffer at room temperature. AP signal was detected using NBT/BCIP tablets (Roche) for 4 h at 30° in darkness. Finally, sections were counterstained with fast red (Sigma), washed in MQ, dehydrated through a graded ethanol series and mounted with entellan (EMS).

Western blotting

Tissue was homogenized in RIPA buffer; phosphatase (Sigma) and protease (Complete®, Roche) inhibitors were added. Lysates were resolved by SDS–PAGE and immunoblotted for SPI1/PU.1 (Cell Signaling Technology, Leiden, the Netherlands) overnight at 4°C. GAPDH (Fitzgerald Industries, Huissen, the Netherlands) was used as a loading control. Imaging was performed on a ChemiDoc XRS+ System (BioRad, Temse, Belgium). Quantification was done using Image J software (NIH).

RNA isolation and expression

RNA was isolated with the miRVana kit (Ambion, Gent, Belgium). We controlled its integrity and concentration using Nanodrop (ThermoScientific, Erembodegem, Belgium) and BioAnalyzer (Agilent, Diegem, Belgium). For murine samples, 1 μg of total RNA was reverse transcribed with the miScript cDNA synthesis kit (Qiagen, Venlo, the Netherlands); for human samples, 0.5 μg of total RNA was reverse transcribed. Real-time quantitative PCR was performed with SYBR green mix (Applied Biosystems, Gent, Belgium) on an ABI Prism 7500 (Applied Biosystems). LNA primers (Exiqon, Vedbaek, Denmark) were used to detection mature miRs. U6 was used as an endogenous control for miRs; GAPDH was used as a housekeeping gene for mRNAs.

MiR and mRNA expression profiling

Total RNA from human biopsies was subjected to miR expression profiling on NanoStrings' nCounter platform by the Nucleomics Core of the Flemish Institute of Biotechnology (Merelbeke, Belgium). The gene target list consisted of 654 human miRs, 80 human-associated viral miRs, 6 positive controls, 8 negative controls, and 5 housekeeping genes. Further identification of differentially regulated miRs was performed using the R pipeline provided by the manufacturer.

Total RNA from mouse hearts was hybridized to mouse miRNA microarray G4472B (Agilent) based on miRBase release 12.0, containing 627 mouse

miRs, 39 mouse viral miRs, 6 negative controls, 6 positive controls, and 5 housekeeping genes. Further identification of differentially regulated miRs was performed using software provided by the manufacturer at Hannover Medical School (MHH, Hannover, Germany).

Total RNA from human biopsies and mouse hearts was subjected to mRNA expression profiling on Affymetrix Human PrimeView and Mouse MoGene 1.0 ST v1 microarrays, respectively. The expression data was normalized using the Affymetrix R package and appropriate CustomCDFs from the Microarray Lab (University of Michigan) (19). Differential expression was assessed in R software(20) using the *limma* package (21).

MiRs were considered differentially expressed with a p-value of <0.05; mRNAs were considered differentially expressed with a p-value of <0.05 and a fold change of >2.0.

Design, synthesis, and application of antagomiR-155 and scram-antagomiR

AntagomiRs were synthesized by Fidelity Systems (Gaithersburg, MD) (22). The antagomiR-155 (anti-155) oligonucleotide 5′-$c_sc_s$ccuaucacaauuagcau$_s$u-$_{sas}a_s$-Chol-3′ is complementary to nucleotides 4-25 in mmu-miR-155. The scrambled antagomiR (anti-scram) has the following sequence: 5′-u_sc_su-gacccuaaacauucaa$_sc_su_sa_s$-Chol-3′. Letters represent 2′-O-Me-modified nucleotides; subscript 's' represent a phosphorothioate linkage; 'Chol' represents cholesterol linked through a hydroxyprolinol linkage.

Statistical analysis

Data are expressed as mean ± SEM. Normal distribution of continuous variables was tested with the Kolmogorov–Smirnov method. An unpaired Student's t test was used when groups passed the normality test, otherwise, a Mann–Whitney test was used. ANOVA with Bonferroni posthoc analysis was performed when more than two groups were compared. Graft outcome data were compared by the log rank test. A two-sided p-value of <0.05 was considered statistically significant.

Results

MiR expression profile in murine and human ACR following HTX

We compared miR expression in human biopsies from control hearts (n = 7) and surveillance EMBs manifesting severe rejection (ISHLT 3; n = 7), from patients during the first year following HTX (Figure 1A).

Microarray analysis identified 47 significantly differentially regulated miRs in EMBs with severe rejection compared with control biopsies, of which 20 were upregulated and 27 downregulated; unsupervised clustering of samples based on miR expression results in perfect discrimination of

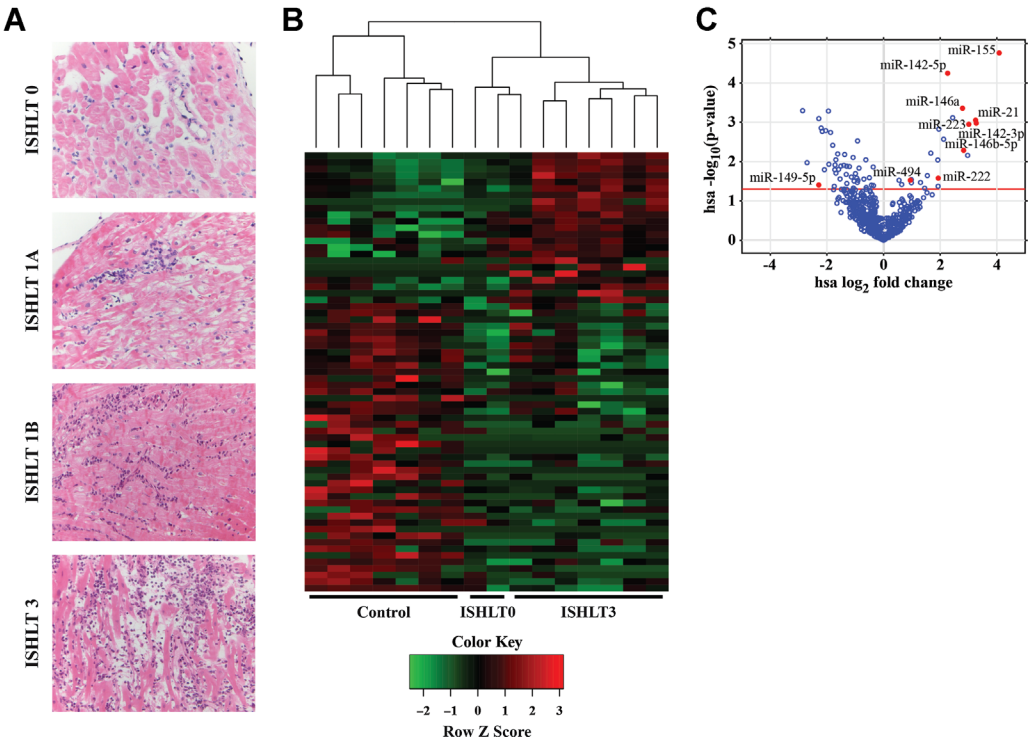

Figure 1: ACR of human cardiac allografts. (A) Hematoxylin-eosin staining of human EMBs manifesting different grades of rejection (ISHLT 0 = no rejection; ISHLT 1 = mild rejection; ISHLT 3 = moderate to severe rejection). (B) Heat map of differentially expressed miRs in control hearts and ISHLT 3 grafts. (C) Volcano plot showing fold change (log_2 values) and probability (log_{10} values) for individual miRs, comparing control and ISHLT 3 hearts. Common dysregulated miRs in humans and mice are highlighted. ACR, acute cellular rejection; EMB, endomyocardial biopsy; ISHLT, International Society of Heart and Lung Transplantation.

control and ISHLT 3 samples (Figure 1B and C; Table S1). Pathway analysis revealed that the 47 dysregulated human miRs have previously been implicated in cancer (both *in situ* growth and metastasis), inflammation, and autoimmune disorders (Table S2).

In parallel, we studied differential miR expression in murine ACR using a full MHC haplotype-mismatched model of HTX involving male BALB/cJ hearts (MHC haplotype H-2^d) to male C57Bl/6J mice (H-2^b)(Figure 2A). In the absence of immunosuppression, graft failure, defined as the cessation of beating of the graft, occurred on the seventh postoperative day (Allo 7d) while inflammation was already present at postoperative day 3 (Allo3d; Figure 2B–E). Cardiac miR expression profiles were analyzed in Allo3d and Allo7d grafts. Here, 173 miRs were differentially regulated in Allo7d versus untransplanted BALB/cJ hearts, of which 86 were upregulated and 87 were downregulated (Figure 2F and G; Table S3). These dysregulated miRs have previously been implicated in the pathogenesis of infectious diseases, diabetes mellitus, and nonalcoholic fatty liver disease (Table S4).

Subsequently, we compared murine and human miR expression profiles of ACR. Our analysis revealed 10 consistently differentially regulated miRs in both species: miR-21, miR-146a, miR-146b, miR-155, miR-142-3p, miR-142-5p, miR-222, miR-223, and miR-494 (consistently upregulated), and miR-149-5p (consistently downregulated) (Figure 2I and J; Table 1). We validated their differential expression by qPCR in mice and humans. In mice, we compared control hearts, Allo3d and Allo7d grafts; qPCR results were in line with the microarray expression profiles and proved the time-dependent change in the expression of the 10 miRs, paralleling the severity of inflammation (Figure S1). In humans, we compared EMBs manifesting ISHLT 0, 1, and 3 rejection for validation qPCRs ($n = 19$, 20, and 10, respectively; Table S5 summarizes patient characteristics). Validation qPCRs revealed that miRs previously linked to inflammation paralleled histopathological ACR severity (miR-142-3p, miR-142-5p, miR-146a, and miR-155) or were able to separate EMBs with rejection from those without ACR (miR-223) (Figure S2).

In conclusion, cardiac ACR induced distinct changes in miR expression in murine and human grafts. MiR-155 is upregulated in human and murine ACR, and the most upregulated miR in human grafts manifesting rejection.

mRNA expression profile in murine and human ACR following HTX

Apart from miR profiling, we performed comparative mRNA arrays in both human and murine control hearts and rejected cardiac allografts. Only transcripts with a significant twofold up or downregulation in rejected allografts were considered differentially expressed. This analysis revealed 70 commonly differentially regulated mRNAs. Remarkably, several highly upregulated common mRNAs in Allo7d grafts were already significantly upregulated in Allo3d grafts. For example, TCRα subunit constant gene (Trac), the most differentially expressed gene in Allo7d grafts, was already 3.6-fold upregulated in Allo3d grafts. Other examples include Cxcl9 and -10, the Guanylate-binding proteins (Gbp) 1 to −5, transporter associated with antigen processing (Tap) 1, CD74, and Stat1, all of which are involved in immune signaling. Upstream regulator and mechanistic network analysis revealed that 33/70 common transcripts are involved in downstream signaling of IL-6 and its transcription factor SPI1 (Figures 3 and 4; Table S6–8). Interestingly, SPI1 has a conserved binding site for miR-155 in its 3′ UTR (18).

In conclusion, ACR induced transcripts involved in immune signaling and immune-related diseases. Specifically, components of the IL-6 signaling pathway including the miR-155 target SPI1 were similarly dysregulated in human and murine ACR.

Genomic absence of miR-155 in cardiac inflammatory cells attenuates ACR

We performed *in situ* hybridization (ISH) on sections of murine inflamed Allo7d grafts to identify which cells produce miR-155 during ACR. We observed perinuclear miR-155 staining in pericardial inflammatory patches and infiltrating cells, whereas we did not detect any signal in adjacent cardiomyocytes (Figure 2H). These findings are in line with previous studies showing miR-155 upregulation in leukocytes following activation (16,18,23).

To support the pathogenic role of miR-155 in ACR, we transplanted BALB/cJ hearts into C57Bl/6J mice with a targeted deletion of miR-155 (miR155−/−) and into their WT littermates (miR155+/+) (Figure 5A). Median graft survival time increased significantly in miR155−/− versus miR155+/+ mice (miR-155−/−: 10 days; miR-155+/+: 7.5 days; $p = 0.004$) (Figure 5B). Despite longer exposure to the recipient's immune system and ensuing tissue edema, grafts from miR155−/− mice weighed significantly less upon rejection (miR-155−/−: 10.1 mg/g ± 1.2; miR-155+/+: 12.7 mg/g ± 1.7; $p = 0.03$) (Figure 5C). However, the amount of infiltrating inflammatory cells in these failed grafts, harvested at different postoperative time points, showed no significant between genotype difference ($p = 0.6$) (Figure S3A).

In another cohort, we sacrificed all animals on postoperative day (POD) 5 (i.e. before occurrence of graft failure) (Figure 5D). Gravimetric analysis showed a numerically lower normalized graft and spleen weight in miR155−/− recipients, yet these differences did not reach statistical significance (grafts, miR155−/−: 5.3 mg/g ± 0.4 vs. miR155+/+: 6.2 mg/g ± 0.6, $p = 0.2$; spleens, miR-155−/−: 4.6 mg/g ± 0.6 vs. miR155+/+: 5.6 mg/g ± 0.5; $p = 0.3$) (Figure S3B and C). More importantly, influx of CD45-positive leukocytes and

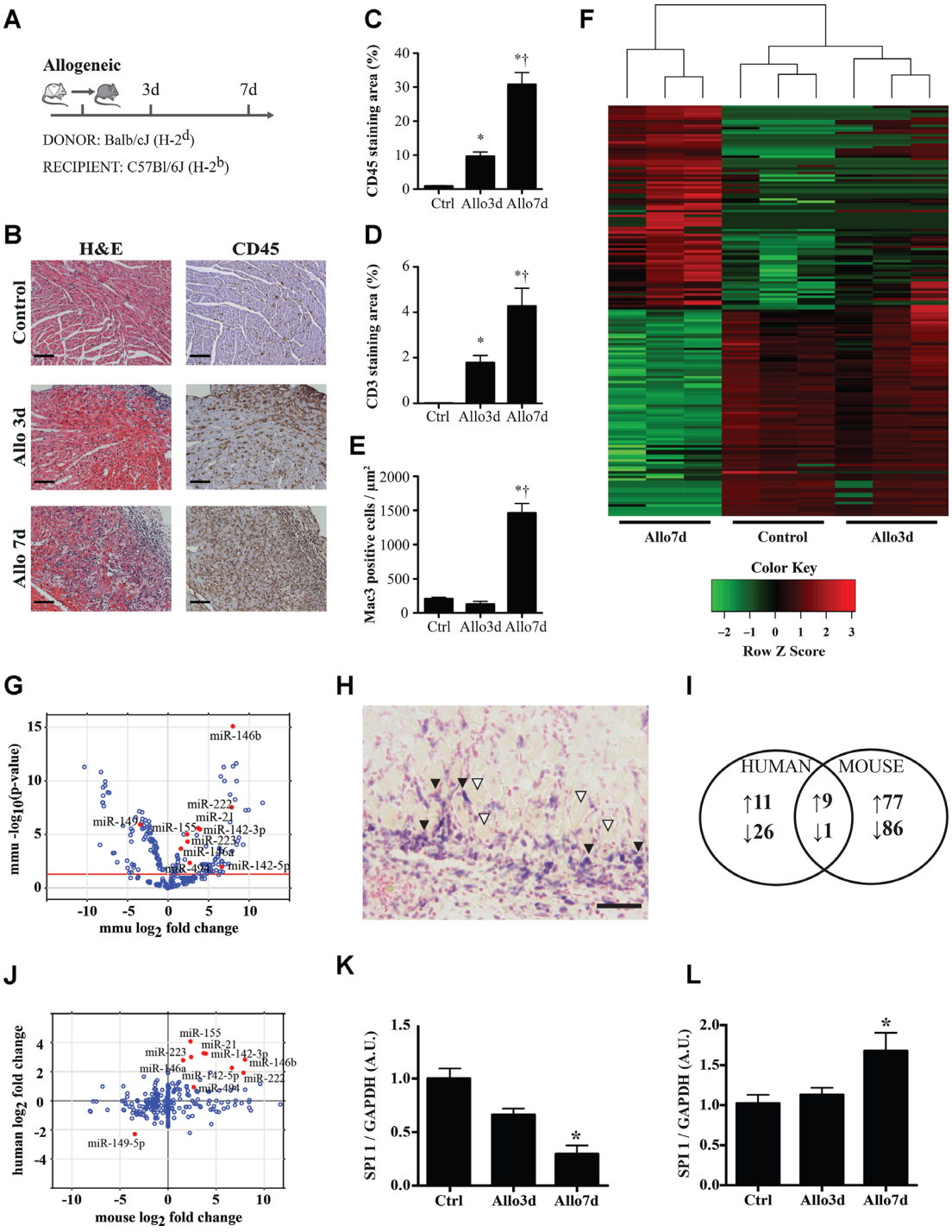

Figure 2: ACR of murine cardiac allografts and comparison of human and murine array results. (A) Schema of included groups to study the murine miR expression profile in ACR following HTX. (B) Representative CD45 staining of corresponding regions in control hearts and cardiac allografts, 3d (Allo3d) and 7d (Allo7d) after HTX, with quantification in (C). (D and E) depict CD4 and Mac3 staining, respectively. (F) Heat map of differentially expressed miRs in murine control hearts and failed grafts. (G) Volcano plot showing fold change (log_2 values) and probability (log_{10} values) for individual miRs, comparing control hearts and Allo7d. (H) ISH of miR-155 during murine ACR showed miR-155 staining in inflammatory cells (black arrowheads), whereas adjacent ventricular myocardium didn't stain (white arrowheads). (I) Venn diagrams showing the numbers and overlap of differentially regulated miRs between humans and mice. (J) Fold changes for all miRs in humans and mice during ACR; common dysregulated miRs in humans and mice during ACR are highlighted. (K) Following HTX, splenic SPI1 protein levels markedly decreased, whereas splenic RNA levels significantly increased (L) (*$p < 0.05$). ACR, acute cellular rejection; HTX, heart transplantation.

Table 1: Ten differentially regulated miRs in mice and humans during ACR

	Homo sapiens		*Mus musculus*	
	Fold change ISHLT 3 versus control	p-value	Fold change Allo 7d versus control	p-value
miR-155	16.95	$9.38\ 10^{-5}$	5.57	$1.77\ 10^{-5}$
miR-146a	6.91	$9.71\ 10^{-4}$	3.42	$1.96\ 10^{-4}$
miR-21	9.67	$1.39\ 10^{-3}$	10.20	$7.72\ 10^{-6}$
miR-142-5p	4.80	$1.48\ 10^{-3}$	13.54	$2.99\ 10^{-5}$
miR-223	8.06	$6.00\ 10^{-3}$	5.19	$2.14\ 10^{-4}$
miR-142-3p	9.51	$6.65\ 10^{-3}$	11.57	$2.55\ 10^{-5}$
miR-146b	7.10	$1.99\ 10^{-2}$	255.71	$7.83\ 10^{-12}$
miR-222	3.81	$2.47\ 10^{-2}$	230.26	$1.83\ 10^{-3}$
miR-494	1.93	$2.66\ 10^{-2}$	9.58	$5.94\ 10^{-4}$
miR-149	0.20	$4.57\ 10^{-2}$	0.10	$1.25\ 10^{-5}$

ACR, acute cellular rejection; ISHLT, International Society of Heart and Lung Transplantation; miR, microRNA.

Mac3-positive macrophages was significantly impaired in BALB/c hearts transplanted into miR155−/− recipients as opposed to miR155+/+ recipients ($p = 0.03$ and 0.04, respectively). CD3-positive area (T cells) was numerically lower in grafts transplanted into miR155−/− recipients, yet this didn't reach statistical significance ($p = 0.3$) (Figure 5E).

Taken together, these results indicate that higher leukocytic expression levels of miR-155 are associated with increasing numbers of infiltrating leukocytes in general and macrophages more specifically.

AntagomiR-155 treatment inhibits acute cardiac allograft rejection

We inhibited miR-155 *in vivo* using three injections of antagomiR-155 (anti-155) targeting mature mmu-miR-155 and compared its beneficial effects with antagomiR-scrambled oligonucleotide (anti-scram) injected recipients. Intravenous injections were administered 1 day before scheduled transplantation and on POD 1 and 3. These time points were arbitrarily chosen to simulate perioperative treatment as could be applied in patients. Mice were sacrificed on POD 5 (Figure 6A).

In unoperated mice, cardiac miR-155 levels, known to be very low in healthy hearts, did not decrease significantly following anti-155 treatment; however, splenic levels decreased significantly (Figure 5C). In transplanted animals, miR-155 levels decreased significantly both in cardiac allografts and spleens upon anti-155 treatment (Figure 6B and C). Biometrical analysis revealed significantly lower graft weights in anti-155 treated mice on POD 5 (anti-scram: $4.8\,mg/g \pm 0.1$; anti-155: $4.0\,mg/g \pm 0.2$; $p = 0.02$) (Figure 6D). More importantly, CD45 staining area decreased significantly following anti-155 treatment, as did the number of Mac3-positive cells infiltrating the graft (Figure 6E and F). Though numerically lower, CD3-positive

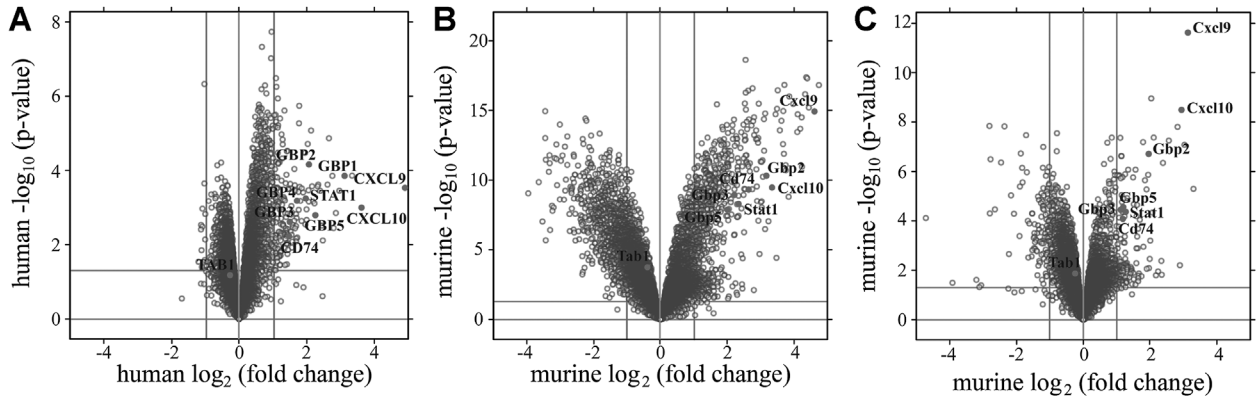

Figure 3: ACR of human and murine cardiac allografts: mRNA array results. (A) Volcano plot showing fold changes (log_2 values) and probability (log_{10} values) for individual human mRNAs, comparing control and ISHLT3 EMBs. (B) Volcano plot showing fold changes (log_2 values) and probability (log_{10} values) for individual murine mRNAs, comparing control hearts and Allo7d. (C) Volcano plot showing fold changes (log_2 values) and probability values (log_{10}) for individual murine mRNAs, comparing control hearts and Allo 3d. ACR, acute cellular rejection; ISHLT, International Society of Heart and Lung Transplantation; mRNA, messenger RNA.

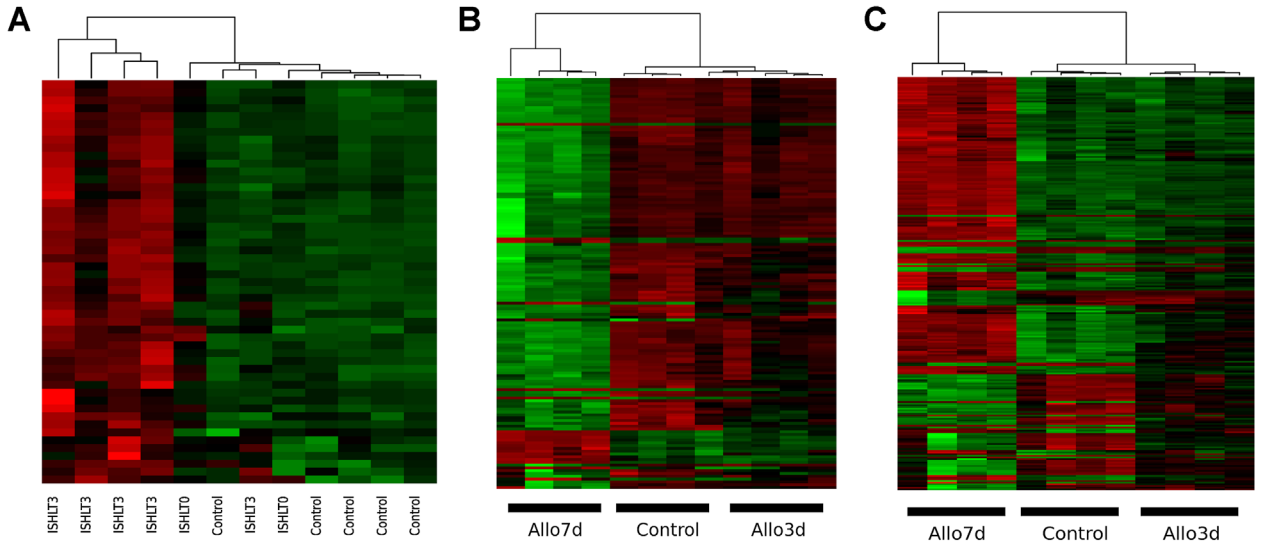

Figure 4: Differentially regulated human and mouse mRNA transcripts from the micro array studies. (A) Pathway enrichment analysis of human mRNA arrays (ISHLT3 vs. control) showed significant enrichment of predominantly immune-related pathways (Table S7). The heat map, showing in rows all genes represented in the enriched pathways, confirm that the ISHLT3 cardiac samples are highly regulated except for one. In addition, gene expression in ISHLT0 cardiac samples does not significantly differ from control gene expression, as becomes apparent from the mixed unsupervised clustering of these groups. (B) Pathway enrichment analysis of murine mRNA arrays (Allo7d vs. control) showed significant enrichment of predominantly metabolic and immune-related pathways (Table S8). The heat maps, showing in rows all genes represented in these pathways, confirm that the Allo7d samples are highly regulated and that the Allo3d samples are in a transition phase in which the respective genes are mildly regulated. Moreover, the unsupervised clustering of the samples based on the gene expression of these pathways results in the perfect discrimination of control, Allo3d, and Allo7d samples. ISHLT, International Society of Heart and Lung Transplantation; mRNA, messenger RNA.

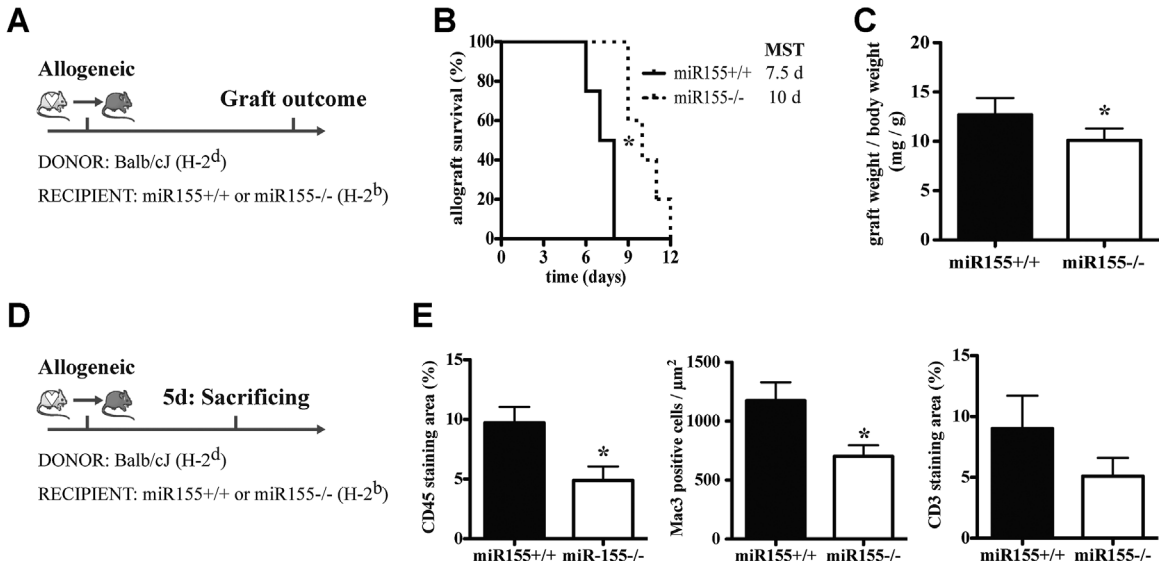

Figure 5: ACR in miR-155 +/+ and miR-155 −/− mice following HTX. (A) Experimental setup of miR-155 +/+ and miR-155 −/− mice in spontaneous survival experiments. (B) Graft failure occurred later when BALB/cJ hearts were transplanted into miR-155 −/− versus miR-155 +/+ mice. (C) Despite longer exposure to the host's immune system, BALB/cJ grafts weighed significantly less when transplanted into miR-155 −/− mice. (D) Experimental setup of miR-155 +/+ and miR-155 −/− mice sacrificed on a fixed time point (5d) following HTX. (E) Whereas the number of infiltrating CD45 and Mac3-positive cells was significantly less in BALB/cJ hearts transplanted into miR155 −/− versus miR-155 +/+ mice, the number of CD3-positive cells did not significantly differ between genotypes (*$p < 0.05$). ACR, acute cellular rejection; MST, median survival time; HTX, heart transplantation; miR, microRNA.

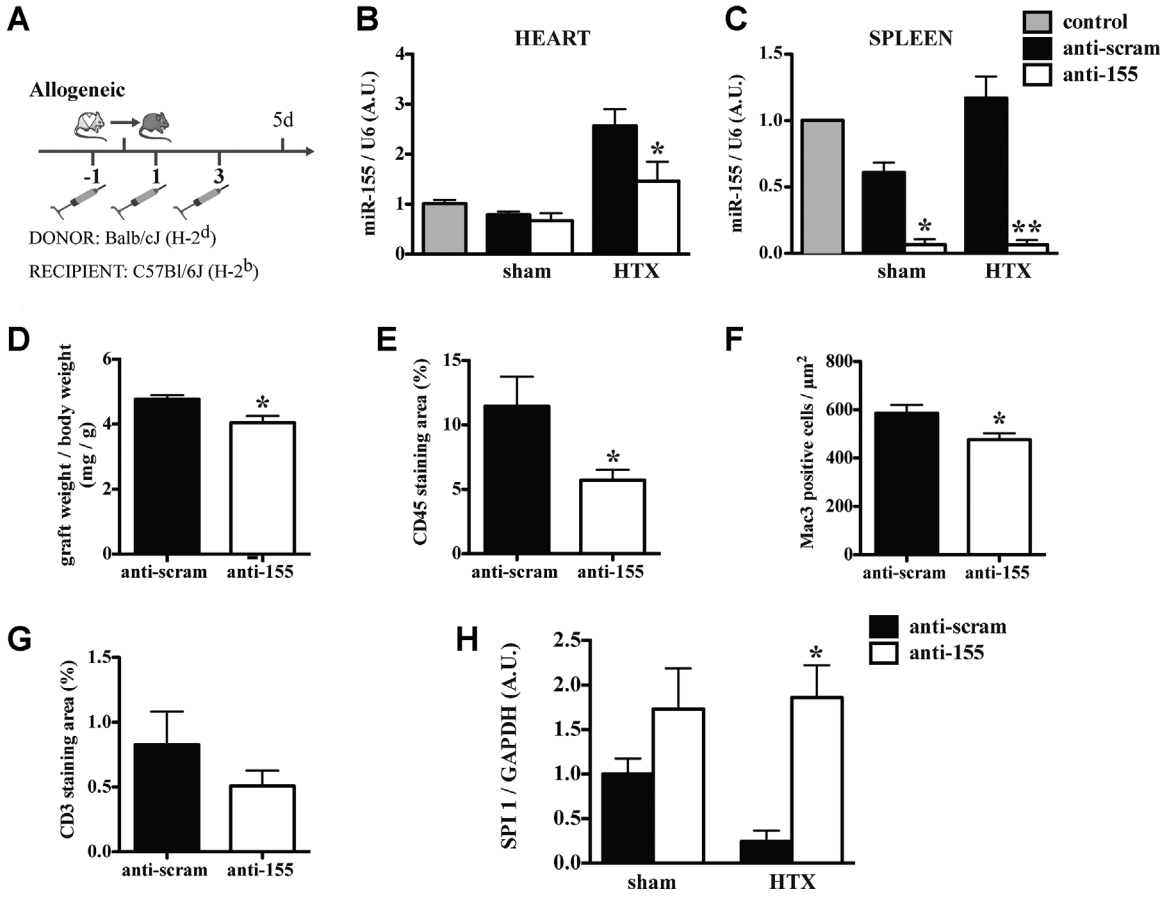

Figure 6: ACR in anti-155 and anti-scram injected mice following HTX. (A) Experimental setup of anti-155 and anti-scram injected mice sacrificed on a fixed time point (5d) following HTX. (B) Normalized expression levels of miR-155 in (un) transplanted hearts following anti-155 and anti–scram injection. (C) Normalized splenic expression levels of miR-155 in (un) transplanted mice following injection with anti-155 and anti-scram. (D) BALB/cJ grafts weighed significantly less when transplanted into anti-155 injected mice. The number of infiltrating CD45 (E) and Mac3-positive (F) cells was significantly less in BALB/cJ hearts transplanted into anti-155 versus anti-scram injected mice. (G) The number of CD3-positive cells was not significantly different between treatments. (H) Following HTX, splenic SPI1 decreased in anti-scram mice, whereas it remained elevated in anti-155 mice. Splenic SPI1 was significantly higher in transplanted anti-155 versus anti-scram injected mice (*$p < 0.05$; **$p < 0.01$). ACR, acute cellular rejection; HTX, heart transplantation.

area in the grafts was not significantly lower in anti-155 treated animals (Figure 5G).

In conclusion, pharmacological miR-155 inhibition was feasible and significantly decreased the number of infiltrating leukocytes and macrophages, which is in line with our results obtained in miR-155−/− mice.

MiRs as a nonorgan specific signature of ACR?

The 10 miRs identified as a common signature of ACR following HTX were also quantified in human renal allograft biopsies. We compared rejecting and nonrejecting samples. Comparable with our observations in cardiac allografts, the subset of five miRs previously implicated in inflammatory processes, miR-142-3p, miR-142-5p, miR-146b, miR-155, miR-223, was able to distinguish between rejecting and nonrejecting samples (Figure 7).

In conclusion, we corroborated our miR hallmark of acute cellular cardiac allograft rejection in acute cellular renal allograft rejection, hinting at a nonspecies and nonorgan specific miR signature of ACR.

Protein levels of miR-155 targets involved in innate immunity decrease during ACR

We quantified the expression of SPI 1 early (Allo3d) and late (Allo7d) after transplantation. SPI 1 is a distinct leukocytic miR-155 target implicated in the repression of IL-6 signaling (24) and acting as an inhibitor of dendritic cell pathogen binding and antigen presentation of dendritic cells to T cells (25). Splenic expression levels of SPI1 decreased in a time-dependent way (Figure 2K). Importantly, RNA levels of SPI1 increased, providing evidence of miR-155's repressive activity with regard to the translation of SPI1 mRNA to protein (Figure 2L).

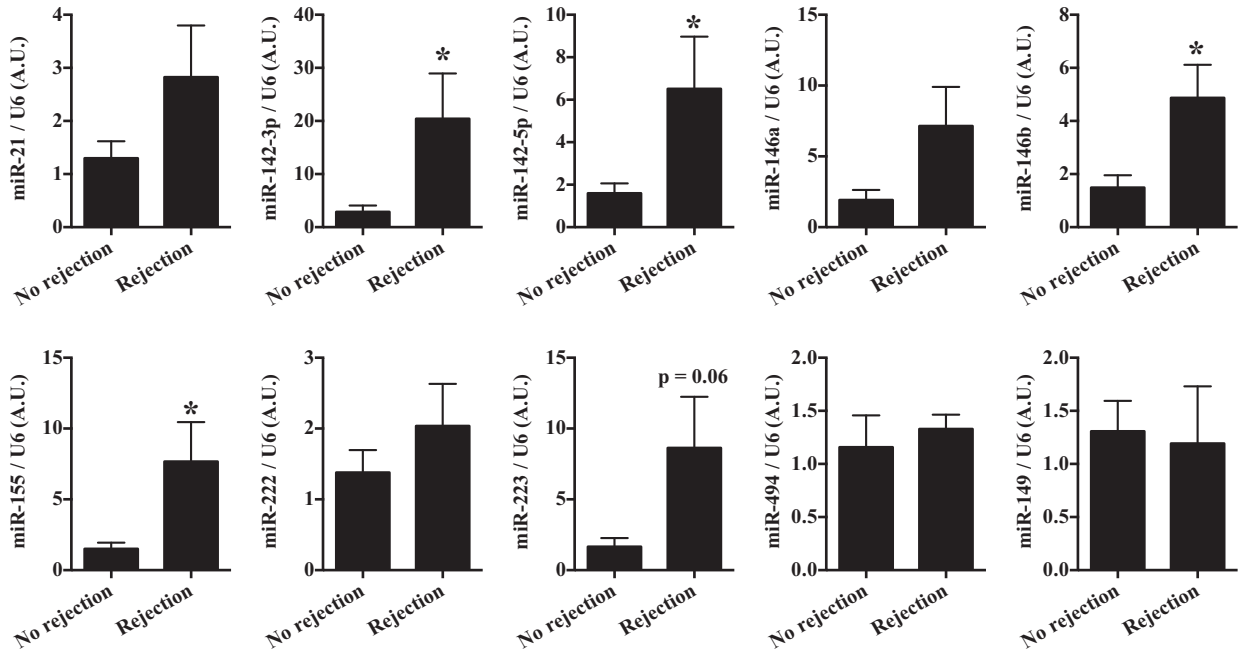

Figure 7: Quantitative RT-PCR validation of miR array results in human rejecting and nonrejecting renal allografts ($p < 0.05$).

Therefore, during ACR, miR-155 may promote antigen presentation by dendritic cells to T cells and stimulate IL-6 signaling by repressing SPI 1, a pivotal inhibitor of these pathways.

To corroborate the decreased influx of inflammatory cells into the allograft following repeated intravenous anti-155 administration and elaborate on the implication of miR-155 in ACR, we compared SPI1 expression in anti-scram and −155 injected animals. Without transplantation, splenic SPI1 levels were similar in both treatment groups ($p = 0.4$). Following cardiac transplantation, splenic SPI1 decreased in anti-scram injected animals, whereas in anti-155 injected mice, SPI1 protein levels remained elevated and significantly higher compared with anti-scram injected mice ($p = 0.03$; Figure 6H).

These data provide evidence for a role of SPI1 and miR-155 during ACR and at the same time demonstrate the feasibility of interfering with miR expression to modulate critical signaling pathways involved in allograft rejection.

Discussion

This study is the first to unravel both miR and mRNA expression profiles in normal hearts and ACR in humans and mice, leading to a miR signature that discriminates rejected from nonrejected grafts. We identify miR-155 as a key contributor to ACR: in humans, miR-155 is the most upregulated miR following rejection and, using an experimental model, we showed that reduced levels of miR-155 attenuated intragraft inflammation and delayed rejection. Apart from establishing miR-155 as a candidate target for novel therapeutics, we provide evidence for a new paradigm to combat rejection, namely by antimiR (18) or antagomiR-based therapeutics.

MiR-155 has an established role in inflammation and immunity (26,27). Macrophage activation and dendritic cell maturation require its upregulation (16,25,28). Furthermore, miR-155 functions at the interface of innate and adaptive immunity as miR-155 deficient dendritic cells are unable to mount appropriate B and T cell responses (14,16,23). These immunological mechanisms all have a pivotal role in ACR. In our study, genomic absence and pharmacological inhibition of miR-155 delayed graft failure by reducing influx of leukocytes (CD45-positive cells) in general and macrophages (Mac3-staining cells) more specifically. In another recent report, antagomiR-155 attenuated allograft rejection through the inhibition of dendritic cell maturation, yet this study did not address miR expression in human transplant samples (14). Taken together, these two studies nonetheless provide evidence for a causal relationship between miR-155 and ACR and the potential of miR-155 targeting to prevent organ rejection.

Apart from miR-155, our miR expression arrays and validation qPCRs revealed additional miRs with comparable changes in human and murine inflamed cardiac grafts: miR-149-5p (downregulated), miR-21, miR-146a, miR-146b, miR-142-3p, miR-142-5p, miR-222, miR-223, and miR494

(upregulated). MiR-142-3p, miR-142-5p, miR-146a, miR-146b, and miR-223 are notorious for their implication in inflammation and the innate immune system (27,29,30). More specifically, upregulation of miR-142-3p, a hematopoietic cell-specific miR, may modulate inflammatory responses to promote graft tolerance, whereas upregulation of miR-142-5p was previously linked to graft rejection (29,31).

Increased miR-21 and miR-222 expression have been implicated in fibrosis (32,33), providing a hypothetical link between ACR and myocardial interstitial fibrosis, a specific manifestation of chronic rejection (1,34). The implication of miR-494 and miR-149-5p in ACR deserves further study. Importantly, TNFα, which increases upon cellular rejection (34), upregulates miR-494 (35) and downregulates miR-149-5p (36), in line with our findings. The upregulation of miR-494 might be beneficial as it prevents ischemia-reperfusion injury (37). The downregulation of miR-149-5p may contribute to the induction of genes downstream of the proinflammatory cytokine IL-6 (38), which we also observed in our mRNA arrays.

Interestingly, others have shown identical miRs as in our study to be changed during ACR of transplanted organs (7,9–13). We, therefore, hypothesize that a generic change in miR expression occurs during ACR, irrespective of the organ transplanted. This generic change, occurring despite contemporary immunosuppressive regimens, merits further study as it hints at common pro-inflammatory pathways in these diverse manifestations of ACR. Admittedly, we restricted our analysis to tissular expression of mRNAs and miRs, whereas others studied their serological expression (7,39). Furthermore, we only compared rejecting and nonrejecting human samples collected during the first year following HTX, the typical ''vulnerable phase'' for ACR, whereas others addressed miR expression around 1 year after transplantation (7). These two caveats may explain why miR expression profiles do not completely overlap between studies.

Our mRNA arrays also revealed interesting new targets to prevent and treat ACR. The comparison of significantly dysregulated transcripts in transplanted mice and patients manifesting rejection yielded 70 common dysregulated mRNAs, with 33 of these 70 coding for proteins involved in the IL-6 pathway. These findings are in line with previous reports on the role of IL-6 in cardiac rejection (40,41) and urge for further efforts to determine the true potential of IL-6 targeting to prevent ACR. Importantly, the pro-inflammatory effects of miR-155 during ACR implicate that it targets mRNAs coding for anti-inflammatory proteins. Intriguingly, our mRNA arrays showed that the 33 dysregulated transcripts involved in the IL-6 pathway also function downstream of SPI1 (18,25) an established target of miR-155. Whereas the anti-inflammatory transcription factor SPI1 decreased during ACR, miR-155 inhibition de-repressed SPI1. We therefore postulate that miR-155 inhibition attenuates allograft rejection partially by de-repression of SPI1, apart from its recently unraveled inhibitory effect on dendritic cell maturation through SOCS1 upregulation (14).

Our study has some limitations. In our derivation cohort, we decided to use untransplanted BALB/cJ hearts as controls rather than BALB/cJ our C57Bl/6J syngeneic grafts. Earlier research indicated that during normal development (42) and following physiological (43) and pathophysiological (44) stimuli applied to the heart, strain-specific differences are undeniable. In addition, we hypothesize that our comparison with human samples intentionally collected beyond 6 weeks after transplant surgery cancels out the inflammatory signature associated with the surgical procedure itself. In retrospect, grafting a BALB/cJ heart into C57Bl/6J Rag $-/-$ common gamma-chain $-/-$ mice would make the optimal control, as this would cancel out the nonimmune inflammatory signature. Furthermore, although we used a sample set of 49 EMBs for validation qPCRs, the scarcity of EMBs manifesting severe rejection in our human cohort obliged us to reuse samples of the derivation cohort in the validation cohort. Future research should validate our markers in an independent set of samples.

In conclusion, ACR induced marked miR and mRNA expression changes in human and murine grafts. MiR-155 was the most upregulated miR during ACR in humans and contributes to adverse cardiac inflammation, as evidenced by prolonged graft survival and diminished leukocyte influx in mice with a targeted genomic deletion of miR-155 and following pharmacological inhibition of miR-155 using antagomiRs. Additional comparison of dysregulated mRNAs in human and murine grafts during ACR-revealed marked induction of genes downstream of the proinflammatory cytokine IL-6 and SPI1, a conserved target of miR-155. As such, this study identifies miRs in general, miR-155 in particular, as well as the IL-6 signaling pathway, as promising targets for the treatment of ACR.

Acknowledgments

L.N.L. Van Aelst is supported by the Research Foundation Flanders, Belgium (FWO-Vlaanderen 1167610N and 1167612N). S. Heymans is supported by the Netherlands Organisation for Scientific Research (Vidi Grant 91796338), the Research Foundation Flanders, Belgium (FWO-Vlaanderen FWO G074009N), the European Union (HOMAGE 305507 for bio-banking and bio-informatics), Marie-Curie Industry Academy Pathways and Partnerships (CARDIOMIR 285991 for array analysis). We acknowledge the support from the Netherlands CardioVascular Research Initiative (CVON2011-11 ARENA).

Disclosure

The authors of this manuscript have no conflicts of interest to disclose as described by the *American Journal of Transplantation*.

References

1. Stehlik J, Edwards LB, Kucheryavaya AY, et al. The Registry of the International Society for Heart and Lung Transplantation: 29th official adult heart transplant report-2012. J Heart Lung Transplant 2012; 31: 1052–1064.
2. Stewart S, Winters GL, Fishbein MC, et al. Revision of the 1990 working formulation for the standardization of nomenclature in the diagnosis of heart rejection. J Heart Lung Transplant 2005; 24: 1710–1720.
3. Miller CA, Fildes JE, Ray SG, et al. Non-invasive approaches for the diagnosis of acute cardiac allograft rejection. Heart 2013; 99: 445–453.
4. Bartel DP. MicroRNAs: Genomics, biogenesis, mechanism, and function. Cell 2004; 116: 281–297.
5. Van Aelst LN, Heymans S. MicroRNAs as biomarkers for ischemic heart disease. J Cardiovasc Trans Res 2013; 6: 458–470.
6. Wei L, Wang M, Qu X, et al. Differential expression of microRNAs during allograft rejection. Am J Transplant 2012; 12: 1113–1123.
7. Duong van Huyen JP, Tible M, Gay A, et al. MicroRNAs as non-invasive biomarkers of heart transplant rejection. Eur Heart J 2014; 35: 3194–3202.
8. Joshi D, Salehi S, Brereton H, et al. Distinct microRNA profiles are associated with the severity of hepatitis C virus recurrence and acute cellular rejection after liver transplantation. Liver Transpl 2013; 19: 383–394.
9. Wilflingseder J, Regele H, Perco P, et al. MiRNA profiling discriminates types of rejection and injury in human renal allografts. Transplantation 2013; 95: 835–841.
10. Scian MJ, Maluf DG, David KG, et al. MicroRNA profiles in allograft tissues and paired urines associate with chronic allograft dysfunction with IF/TA. Am J Transplant 2011; 11: 2110–2122.
11. Anglicheau D, Sharma VK, Ding R, et al. MicroRNA expression profiles predictive of human renal allograft status. Proc Natl Acad Sci USA 2009; 106: 5330–5335.
12. Asaoka T, Sotolongo B, Island ER, et al. MicroRNA signature of intestinal acute cellular rejection in formalin-fixed paraffin-embedded mucosal biopsies. Am J Transplant 2012; 12: 458–468.
13. Sotolongo B, Asaoka T, Island E, et al. Gene expression profiling of MicroRNAs in small-bowel transplantation paraffin-embedded mucosal biopsy tissue. Transplant Proc 2010; 42: 62–65.
14. Gao Y, Liu F, Zhou Q, et al. Mir-155 regulates cardiac allograft rejection by targing the expression of suppressor of cytokine signaling-1 (DOCS1) in dendritic cells. Int J Clin Exp Med 2014; 7: 4572–4583.
15. Chen ZH. A technique of cervical heterotopic heart transplantation in mice. Transplantation 1991; 52: 1099–1101.
16. Rodriguez A, Vigorito E, Clare S, et al. Requirement of bic/microRNA-155 for normal immune function. Science 2007; 316: 608–611.
17. Heymans S, Luttun A, Nuyens D, et al. Inhibition of plasminogen activators or matrix metalloproteinases prevents cardiac rupture but impairs therapeutic angiogenesis and causes cardiac failure. Nat Med 1999; 5: 1135–1142.
18. Corsten MF, Papageorgiou A, Verhesen W, et al. MicroRNA profiling identifies microRNA-155 as an adverse mediator of cardiac injury and dysfunction during acute viral myocarditis. Circ Res 2012; 111: 415–425.
19. Dai M, Wang P, Boyd AD, et al. Evolving gene/transcript definitions significantly alter the interpretation of GeneChip data. Nucleic Acids Res 2005; 33: e175.
20. R Development Core Team. R: A language and environment for statistical computing. Vienna, Austria: R Foundation for Statistical Computing; 2014.
21. Smyth GK. Linear models and empirical bayes methods for assessing differential expression in microarray experiments. Stat Appl Genet Mol Biol 2004; 3: Article 3.
22. Krutzfeldt J, Rajewsky N, Braich R, et al. Silencing of microRNAs in vivo with 'antagomirs'. Nature 2005; 438: 685–689.
23. Thai TH, Calado DP, Casola S, et al. Regulation of the germinal center response by microRNA-155. Science 2007; 316: 604–608.
24. Sun Y, Sun J, Tomomi T, et al. PU.1-dependent transcriptional regulation of miR-142 contributes to its hematopoietic cell-specific expression and modulation of IL-6. J Immunol 2013; 190: 4005–4013.
25. Martinez-Nunez RT, Louafi F, Friedmann PS, Sanchez-Elsner T. MicroRNA-155 modulates the pathogen binding ability of dendritic cells (DCs) by down-regulation of DC-specific intercellular adhesion molecule-3 grabbing non-integrin (DC-SIGN). J Biol Chem 2009; 284: 16334–16342.
26. Faraoni I, Antonetti FR, Cardone J, Bonmassar E. MiR-155 gene: A typical multifunctional microRNA. Biochim Biophys Acta 2009; 1792: 497–505.
27. O'Connell RM, Rao DS, Chaudhuri AA, Baltimore D. Physiological and pathological roles for microRNAs in the immune system. Nat Rev Immunol 2010; 10: 111–122.
28. O'Connell RM, Taganov KD, Boldin MP, Cheng G, Baltimore D. MicroRNA-155 is induced during the macrophage inflammatory response. Proc Natl Acad Sci USA 2007; 104: 1604–1609.
29. Danger R, Paul C, Giral M, et al. Expression of miR-142-5p in peripheral blood mononuclear cells from renal transplant patients with chronic antibody-mediated rejection. PLoS ONE 2013; 8: e60702.
30. Labbaye C, Testa U. The emerging role of MIR-146A in the control of hematopoiesis, immune function and cancer. J Hematol Oncol 2012; 5: 13.
31. Danger R, Pallier A, Giral M, et al. Upregulation of miR-142-3p in peripheral blood mononuclear cells of operationally tolerant patients with a renal transplant. J Am Soc Nephrol 2012; 23: 597–606.
32. Kumarswamy R, Volkmann I, Thum T. Regulation and function of miRNA-21 in health and disease. RNA Biol 2011; 8: 706–713.
33. Shen WJ, Dong R, Chen G, Zheng S. MicroRNA-222 modulates liver fibrosis in a murine model of biliary atresia. Biochem Biophys Res Commun 2014; 446: 155–159.
34. Vanhoutte D, van Almen GC, Van Aelst LN, et al. Matricellular proteins and matrix metalloproteinases mark the inflammatory and fibrotic response in human cardiac allograft rejection. Eur Heart J 2013; 34: 1930–1941.
35. Lee H, Jee Y, Hong K, Hwang GS, Chun KH. MicroRNA-494, upregulated by tumor necrosis factor-alpha, desensitizes insulin effect in C2C12 muscle cells. PLoS ONE 2013; 8: e83471.
36. Palmieri D, Capponi S, Geroldi A, Mura M, Mandich P, Palombo D. TNFalpha induces the expression of genes associated with endothelial dysfunction through p38MAPK-mediated down-regulation of miR-149. Biochem Biophys Res Commun 2014; 443: 246–251.
37. Wang X, Zhang X, Ren XP, et al. MicroRNA-494 targeting both proapoptotic and antiapoptotic proteins protects against ischemia/reperfusion-induced cardiac injury. Circulation 2010; 122: 1308–1318.
38. Clay CC, Maniar-Hew K, Gerriets JE, et al. Early life ozone exposure results in dysregulated innate immune function and altered microRNA expression in airway epithelium. PLoS ONE 2014; 9: e90401.
39. Pham MX, Teuteberg JJ, Kfoury AG, et al. Gene-expression profiling for rejection surveillance after cardiac transplantation. New Engl J Med 2010; 362: 1890–1900.

40. Iida S, Omoto K, Kanemitsu I, et al. Interleukin-6 receptor signaling disruption prevents cardiac allograft deterioration in mice. Exp Clin Transplant 2012; 10: 375–385.
41. Booth AJ, Grabauskiene S, Wood SC, Lu G, Burrell BE, Bishop DK. IL-6 promotes cardiac graft rejection mediated by CD4+ cells. J Immunol 2011; 187: 5764–5771.
42. Kahr PC, Piccini I, Fabritz L, et al. Systematic analysis of gene expression differences between left and right atria in different mouse strains and in human atrial tissue. PLoS ONE 2011; 6: e26389.
43. Lerman I, Harrison BC, Freeman K, et al. Genetic variability in forced and voluntary endurance exercise performance in seven inbred mouse strains. J Appl Physiol 2002; 92: 2245–2255.
44. van den Borne SW, van de Schans VA, Strzelecka AE, et al. Mouse strain determines the outcome of wound healing after myocardial infarction. Cardiovasc Res 2009; 84: 273–282.

Supporting Information

Additional Supporting Information may be found in the online version of this article.

Figure S1: **Quantitative RT-PCR validation of miR array results in murine cardiac allografts**.

Figure S2: **Quantitative RT-PCR validation of miR array results in human cardiac allografts.**

Figure S3: **Acute cellular rejection in miR-155 +/+ and miR-155 −/− mice following HTX.**

Table S1: Differentially regulated human miRs in ISHLT3 versus Control.

Table S2: Ingenuity Pathway Analysis of differentially regulated human miRs in ISHLT3 versus Control EMBs.

Table S3: Differentially regulated mouse miRs in Allo7d versus Control.

Table S4: Ingenuity Pathway Analysis of differentially regulated mouse miRs in Allo7d versus Control.

Table S5: Patient characteristics in validation cohort.

Table S6: Differentially regulated human and mouse mRNA transcripts from the micro array studies.

Table S7: Pathway analysis of differentially regulated human mRNAs in ISHLT 3 versus Control EMBs.

Table S8: Pathway analysis of differentially regulated mouse mRNAs in ACR.